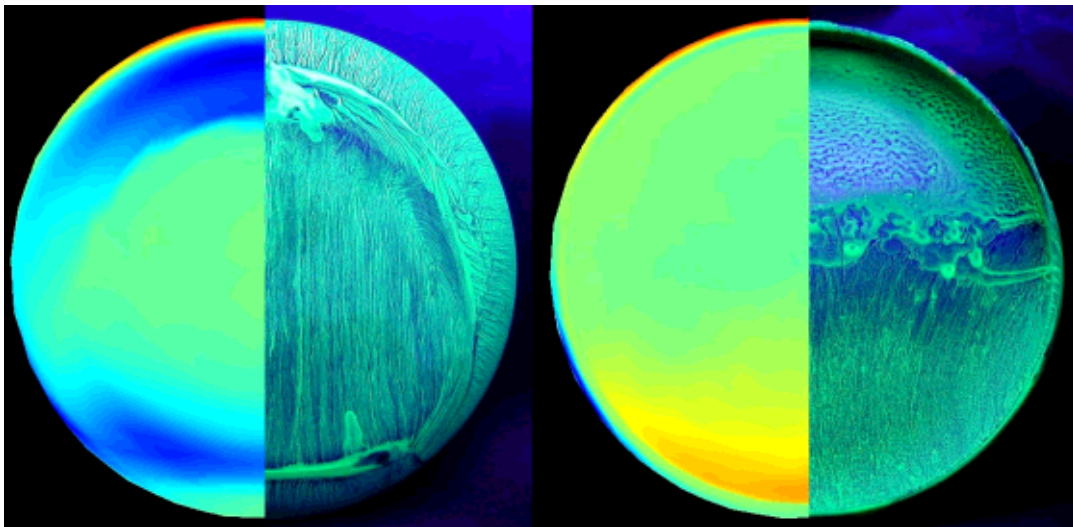




AIAA 2002-3150

FrisbeeTM Aerodynamics

J.R. Potts & W.J. Crowther
Fluid Mechanics Research Group
University of Manchester, UK



20th AIAA Applied Aerodynamics Conference & Exhibit

24 – 26 June 2002

St. Louis, Missouri

For permission to copy or to republish, contact the copyright owner
named on the first page.

For AIAA-held copyright, write to AIAA Permissions Department,
1801 Alexander Bell Drive, Suite 500, Reston, VA, 20191-4344.

FRISBEE™ AERODYNAMICS

Jonathan R. Potts* & William J. Crowther†
 Fluid Mechanics Research Group, School of Engineering,
 University of Manchester, U.K.

Abstract

The frisbee-like flying sports disc is a spin-stabilised axi-symmetric wing of quite remarkable design. The disc generates lift through forward velocity just like a conventional wing. From a backhand throw, spin is naturally given to the disc, which stabilises it in free-flight. This experimental investigation of a typical flying disc shape outlines wind-tunnel data including plots of aerodynamic loads versus angle of attack (AoA) which are compared to existing data in the literature, the effect of spin is also presented. The surface pressure distribution is presented as pressure profiles at the halfspan station and colour filled contour plots for both the upper and cavity surfaces. Surface and smoke wire flow visualisation techniques provide an explanation of flow structures which compare well with the pressure distributions. The asymmetries observed in the trailing vortices, for a spinning disc, allow an explanation of the aerodynamic generation of the rolling moment and side force. The free-flight of a flying disc is discussed based on the above.

Nomenclature

| | |
|----------|--|
| AdvR | Advance ratio ($\Omega\pi c / V$) |
| AoA | Angle of attack ($^\circ$) |
| AR | Aspect ratio |
| cg | Centre of gravity |
| cp | Centre of pressure |
| C_L | Lift coefficient |
| C_D | Drag coefficient |
| C_{D0} | Profile drag coefficient |
| C_Y | Side force coefficient |
| C_M | Pitching moment coefficient (about $c/2$) |
| C_R | Rolling moment coefficient |
| C_p | Pressure coefficient |

| | |
|----------|---|
| c | Disc-wing chord & diameter (m) |
| g | Acceleration due to gravity (ms^{-2}) |
| L | Lift (N) |
| Re | Reynolds number |
| t | Disc thickness (m) |
| V | Wind velocity (ms^{-1}) |
| x,y,z | Roll, pitch, yaw axes |
| p,q,r | Rates of roll, pitch, yaw (rad s^{-1}) |
| R,M,N | Rolling, pitching, yawing moments (Nm) |
| Ω | Spin rate (Hz) |

Introduction

In its simplest form a flying disc can be described as an axi-symmetric flat plate or a cylinder of approximately zero height but is more broadly defined as a circular planform lifting surface. A spin-stabilised flying disc is most commonly encountered as a Frisbee™ sports disc or a Discus in field athletics. The disc considered in this study has an approximate elliptical cross-section and hollowed out underside cavity, characteristic of a Frisbee-like configuration. ‘Disc-wing’ is another term used to describe a flying disc.

History of Frisbee™ Disc

William Russell Frisbie moved to Bransford, Connecticut, USA where he began to manage a branch of the Olds Baking Company in 1871. His success led to buying the bakery to form the Frisbie Pie Company, increasing production to supply a number of East Coast shops. It is this humble pie making family from which the Frisbee™ derives not only its name but the basic shape also. There is some dispute as to whether Cookie-tin lids or Pie-tins were thrown as the first prototype but the commercial value was realised thereafter with the birth of plastic in the 1940’s and growing interest in flying saucers from outer space.

Walter Frederick Morrison of West Coast USA bought an injection mould in the late 1940’s and began production of his first flying disc design. His first design was the somewhat brittle Morrison’s Flyin’ Saucer disc which had a tendency to shatter on impact with a hard surface. His superior design, the Sputnik,

* Research Student, Goldstein Res. Lab., Student Member AIAA.

† Lecturer, Division of Aerospace Engineering.

Copyright © 2002 by J.R.Potts. Published by the American Institute of Aeronautics and Astronautics Inc. with permission.

[i] ‘Frisbee-like’ is used to define the aerodynamic shape of the generic flying disc-wing model tested in this study, for ease of description and understanding. Frisbee™ is a registered trademark of Wham-O Inc.

flew much more successfully and became the inspiration for all subsequent Frisbee™ designs.

Rich Knerr and A. K. Melin started a toy company on leaving the University of Southern California in the early 1950's. They saw Morrison's Flying Saucers thrown on Californian beaches and targeted Morrison in 1955 making him a proposition to increase production. In 1957 the Wham-O Pluto Platter was sold across the US and succeeding models became collectively labelled Frisbee™ after the misspelling of the original Frisbie pie family.

Many flying disc related sports were birthed largely during the 1960's with Wham-O's vice president Ed Headrick driving the development of the Professional Frisbee™ Model in 1964 and founding the International Frisbee Association. The Guts Frisbee Championship among other events were initiated during this period; Ultimate Frisbee, probably the most widely played flying disc sport today, was devised in 1969. From small beginnings the flying disc matured from its toy status to become a serious sport implement.

Ed Headrick appears as the inventor of the 'Flying Saucer' on a patent application² granted in 1967, the first of many flying disc designs protected under law. Disc design matured thereafter driven largely by the increasing popularity of Disc Golf, which is much the same idea as (Ball) Golf. Just as the professional golfer has a variety of clubs, the pro-disc golfer carries a number of discs for various situations. For example, a well designed driver disc has minimum drag for maximum range and little tendency to divert from a straight-line trajectory. The distance record currently stands at 250m held by Christian Sandstrom thrown on 26th April 2002 with an Innova™ DX Valkyrie disc.

A more detailed history of the Frisbee™ disc is given in Ref. 1.

Disc-wing Flight Dynamics

As an introduction to the dynamics of disc-wing flight consider Fig. 1a. Note that for a Frisbee-like shape at typical flight angles of attack, the centre of pressure (cp) of the disc-wing is ahead of the centre of the disc i.e. ahead of the disc cg. This results in an untrimmed nose up pitching moment. If the disc is rotating, gyroscopic effects dictate that this pitching moment results in a precessional rolling rate, p . Thus spin provides enhanced pitch stiffness at the expense of roll stability. Using the conventional body fixed axes definition (Figure 1b), for a disc rotating in the direction of positive yaw then a positive pitching moment will generate a negative roll rate.

Literature Review

The flying disc is of fundamental interest to the aerodynamicist, however the peripheral nature of such a shape to mainstream aeronautical applications has ensured that the disc-wing has largely escaped scientific scrutiny. The literature base detailing the aerodynamics

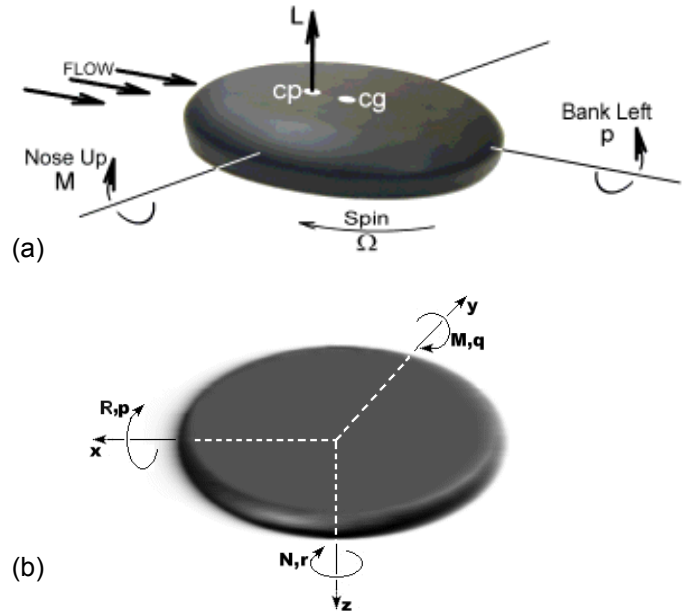


Fig. 1 (a) Disc-wing flight dynamics. (b) Schematic diagram of body fixed axes. N.B. for a conventional aircraft the nose would point in the positive x-direction.

of circular-wing planforms is almost non-existent in comparison to that documenting the delta-wing, for example. The information that is available has been derived from a number of obscure sources and sometimes unpublished reports from inter-related fields such as fluid mechanics, aeronautical engineering & sports engineering. A summary of papers directly related to flying sports disc aerodynamics are reviewed below. The reader is referred to other work by the authors for a review of related documents for aeronautical and aerospace applications, which detail the development of experimental aircraft with circular planform³.

In 1972 the U.S. Navy commissioned a project to further the development of a self-suspended flare, which was essentially a spin-stabilised axi-symmetric flying disc. Stilley & Carstens^{4,5} investigated the aerodynamics of the flare and other similar flying discs. Wind tunnel test results were obtained for a non-spinning Frisbee-like model and published as typical plots of axial, normal and pitching moment coefficients. The effect of spin on the loads was investigated and found to be negligible, for the purposes of their work.

Lazzara et al⁶ outlined a project to develop a wind tunnel balance to measure the aerodynamic loads acting on a frisbee-like flying disc. They presented lift and drag results for various flow speeds, spin rates over a narrow angle of attack range (0° to 10°). They concluded that spin generates a small component of lift.

Mitchell⁷ measured lift and drag for three non-spinning disc-wing configurations and various flow speeds. Ali⁸ measured pitching moment in addition.

Cotroneo⁹ analysed biomechanic and aerodynamic aspects of disc flight from throw observations. Release velocities were correlated with range to conclude that initial velocity is the most important factor affecting the maximum distance thrown.

Lissaman developed a mathematical model of free-flight disc mechanics including static & dynamic aerodynamic terms¹⁰. An investigation of the flight dynamics of a spinning oblate spheroid (disc-wing) involved an analysis to derive stability modes from the characteristic equation¹¹. More recently, he considered the maximum range of a flying disc compared to other well known projectiles¹². Katz¹³ also considered the stability properties of a rotating disc.

Hubbard & Hummel have developed a computer flightpath simulation for a frisbee disc¹⁴ and captured flight trajectories experimentally using high speed cameras¹⁵, to gather dynamic flight data in three-dimensional space. Their research seeks to match simulated flight trajectories to actual free flight data as verification of a realistic computer model. Recent work has studied the human biomechanics of the Frisbee throwing motion¹⁶.

Potts & Crowther investigated the aerodynamics of a flying disc in the wind tunnel^{17&18}. They measured the aerodynamic loads, surface pressure distribution and visualised the flow, using experimental techniques. More recently, they applied aerodynamic control methodologies to a disc-wing to investigate the practicality for unmanned platforms^{3,19&20}.

Independently, Higuchi et al²¹ investigated the flow over a similar disc-wing using smoke wire flow visualisation and PIV (particle image velocimetry) measurements.

Yasuda²² measured the lift and drag characteristics of a flying disc for various flow speeds & spin rates, alongside a flat plate disc.

Nakamura & Fukamachi²³ visualised the flow past a frisbee using the smoke wire method.

Pozzy investigated the correlation of throw speed with range²⁴ and like Cotroneo concluded that there is a relationship between initial velocity and maximum distance thrown. He also investigated throwing technique, analysing high-speed camera footage of disc golf professionals throwing technique²⁵.

In related work, Zdravkovich et al²⁶ studied the aerodynamics of what he called ‘coin-like cylinders’. They have a thickness to chord ratio much less than 1, $t/c \ll 1$, where t is the thickness and c is the chord or diameter of the cylinder. Independent studies by Ganslen²⁷ and Tutjowitsch²⁸ measured the lift & drag characteristics for the discus from field athletics. Kentzer & Hromas²⁹ measured the pitching moment, in addition to the aerodynamic forces.

This paper details an experimental study of flying disc aerodynamics, including both spinning and non-spinning tests, carried out in the wind tunnel. Load measurements, pressure data and flow visualisation techniques have enabled an explanation of the flow physics.

Experimental Methods

The axi-symmetric geometry of the disc-wing dictates that, irrespective of the disc’s orientation to the free stream, the flow over the disc is independent of roll and yaw angle. Which means that the flow speed, angle of attack and the spin rate are the only parameters warranting investigation experimentally. Therefore the flow analysis can be reduced to the wind tunnel testing of a rotating disc-wing at incidence.

Wind Tunnel & Apparatus

The disc-wing model was tested in two low speed wind tunnels: The first had an open-circuit with a test section of 0.9×1.1 m, a top speed of 50m/s and a turbulence level of 0.5%. The second wind tunnel had a closed-circuit with a test section of 2.1×2.7 m, a top speed of 70m/s and a turbulence level of 0.1%. The second tunnel was used for the smoke wire experiments due to the superior flow quality at very low speeds.

A metal frame was used to mount the disc-wing in the wind tunnel (Fig. 2). An L shaped arm mounted the disc vertically on a horizontal axle supported by a vertical strut. The disc was mounted on a motor driven axle to test at various spin rates. The disc’s centre of mass remained at the balance centre at all times.

The disc-wing cross-sectional profile can be seen in Fig. 3a. The disc-wing chord c is equal to the diameter and the thickness t is defined as the maximum perpendicular distance of the cavity lip from the flat

upper surface. The aspect ratio, AR , for a circular planform wing is $4/\pi \approx 1.27$, centre line thickness to chord ratio t/c is 0.14, $c = 0.275\text{m}$.

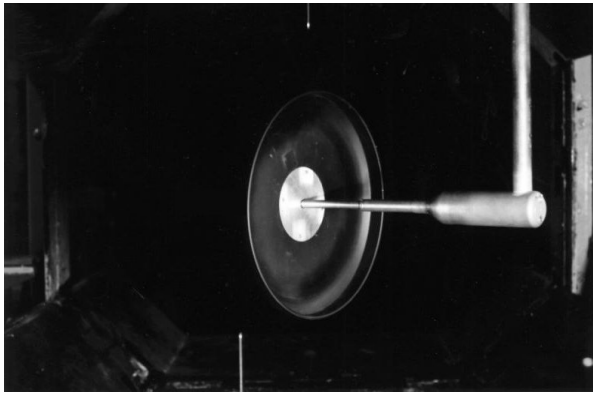


Fig. 2 The L-shaped rig configuration supporting a vertical disc at an AoA.

A number of flying disc models were used for the testing, the frisbee-like configuration (Fig. 3a) for load measurement was made from aluminium, others were produced from a plastic injection mold for use in flow visualisation experiments. Two other discs of different cross-sections were shaped from aluminium plate (Fig. 3b&c).

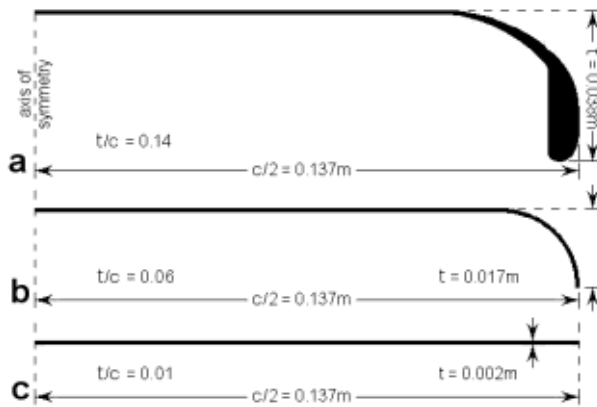


Fig. 3 Cross-sectional flying disc profiles.
(a) Frisbee-like (b) Intermediate (c) Flat Plate.

Load Measurement

The aerodynamic loads acting on the disc were measured using a six component overhead balance. The rig-mounted disc-wing model was tested over a range of Reynolds numbers from 1.13×10^5 to 3.78×10^5 , corresponding to a speed range of 6m/s to 20m/s, with an angle of attack range from -10° to as much as 50° and spin rates up to an advance ratio, ratio of disc rim speed to flow speed ($AdvR$), of 1.

The aerodynamic forces acting on the rig and disc induced mechanical moments due to the off-centre lone strut configuration. This had a significant effect on the pitching and rolling moment measurements. Taking measurements of the moments caused by the static loading of the strut at the centre of the balance, these mechanical components were removed.

Interference and tare effects due to the strut were measured with the disc mounted on a dummy support. The dummy strut was a mirror image of the measuring strut and held the disc in the correct position, on the balance centre.

Surface Pressure Distribution

The surface pressures on a non-rotating disc-wing were measured using a pressure transducer connected via a scanny valve to twenty pressure tappings (Fig. 4) on each side of the disc. Two discs were used to take measurements for the upper and lower surfaces separately, to eliminate strut interference. Tests were performed at 20m/s through an AoA range of -10° to 30° and at 5° for velocities 6, 10, 15 & 20m/s. The tappings were arranged in a curved line extending out from the centre at regular positions along the surface profile. The pressure across the entire disc surface was measured by yawing the model at 12° increments to achieve effective coverage of the entire surface. 1200 measurements in total, for each set of conditions.

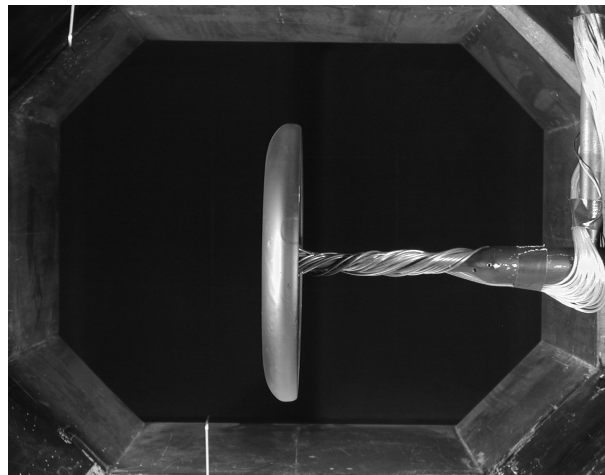


Fig. 4 The L-shaped rig configuration, to measure the pressure distribution on the upper surface.

Flow Visualisation

A film of fluorescent paint, made up of a mix of two parts kerosene to one part fluorescent powder, was applied liberally to the surface of a non-spinning disc. The disc was then placed in the wind tunnel and as the kerosene evaporated the time-averaged surface flow

patterns were revealed. Surface paint patterns were taken for the flow over both the upper and cavity surfaces for a range of incidence angles from 0° to 30° , $V = 15\text{m/s}$, $Re = 2.84 \times 10^5$.

The smoke wire technique was ideal to visualise a complex 3D flow such as this. A vertical wire was mounted upstream of the disc with a pressurised oil reservoir connected allowing continuous feed of droplets to the wire. The wire was electrically heated causing the oil to vaporise producing smoke filaments. The flow field was illuminated using 1000Watt halogen spot lamps positioned on opposite sides of the disc. The cross-sections of the vortex structures were illuminated using a laser light sheet. Footage of the smoke was captured by a video camera operating at various shutter speeds and individual images were transferred to a computer via a frame grabber card.

Experimental Results & Discussion

Load Data

The results for a non-rotating flying disc are presented first, as it is necessary to understand the static case before considering the more complicated spin-stabilised aerodynamics.

The lift and drag trends for a disc-wing are shown in Fig. 5a,b for a Reynolds number, $Re = 3.78 \times 10^5$, equivalent to a flow speed of 20m/s and an AoA (angle of attack) range of -10° to 30° . The linear lift curve (Fig. 5a) and parabolic drag (Fig. 5b) are typical of a low aspect ratio finite wing¹⁷. The lift curve has slope 0.05 per degree and the drag curve shows a minimum profile drag coefficient, C_{D_0} , of 0.085 at the zero lift AoA, -3° . The pitching moment curve (Fig. 5c) is the torque about the half chord position, rather than the more conventional quarter chord position, because this is the location of the centre of gravity. It is non-linear and displays a negative (nose down) coefficient of -0.01 at the zero lift angle of attack (-3°). Zero pitching moment (trim) occurs at 9° AoA and positive (nose up) pitching moment for higher angles.

Previous work by the authors established that the lift and drag characteristics were independent of Reynolds number i.e. the C_L & C_D curves overlay one another for the range of tunnel speeds tested¹⁷. Also, a marked decrease in lift, drag and pitching moment is observed at 45° , which corresponds to the stall AoA³.

Over the years, the flying disc has evolved into the shape depicted in Fig. 3a but why is it successful as a sport implement and recreational toy? A comparison of the frisbee-like shape to a disc with half the thickness

(intermediate) and a flat plate disc is shown in Fig. 6. Using the frisbee-like configuration as the baseline case, the intermediate disc has higher lift (Fig. 6a) and lower drag (Fig. 6b) over the typical flight angle of attack range, 0° to 10° . This would suggest that the aerodynamic performance of the intermediate disc is superior. However take a look at the pitching moment (Fig. 6c), the gradient for the intermediate disc is far higher providing a stronger precessional roll divergence above 3° AoA. This will cause the disc to roll, bank and sideslip away from the intended flight direction more strongly than the frisbee-like disc. The flat plate disc configuration has less lift and drag than the baseline case. The zero lift AoA at 0° (Fig. 6a) is expected due to the symmetric cross-section of the flat plate disc. The C_L slope remains unchanged at 0.05 per degree. The minimum thickness of the flat plate disc ensures that the profile drag is very low, $C_{D_0} = 0.015$ at 0° AoA. The pitching moment is even greater for the flat plate disc, below 16° AoA, and rolls even more strongly, due to precession, than the more cambered shapes tested. The pitching moment curve (Fig. 6c) has a marked decrease in gradient at around 10° AoA. The reduced drag and increased lift of the intermediate shape would suggest superior performance but the larger (nose up) pitching moment would give stronger roll divergence. The profile drag of the flat plate disc is tiny but the pitching moment is even larger than the intermediate disc. The frisbee-like shape is the most favourable for use as a flying sports disc due to the minimum pitching moment gradient for the typical flight AoA range.

A comparison of the aerodynamic loads to data from the literature is shown in Fig. 7, for disc geometries similar to Fig. 3a. The data is derived from three wind tunnel experiments^{4,8&22} and a free-flight experiment¹⁵. The various experiments are in rough agreement, the lift curves (Fig. 7a) all have a negative zero lift AoA and linear gradient, the gradients however show slight variation in magnitude. The parabolic drag curves (Fig. 7b) give good agreement for the profile drag but like the lift curves diverge at higher AoA. Hubbard & Hummel's estimates (based on initial 'short-flight' experiments) of the drag coefficient are far from overlaying the wind tunnel data. The pitching moment curves (Fig. 7c) all show non-linearity, except Hubbard & Hummel's estimates which form a straight line. Stillely & Carstens' show a negative pitching moment, at low AoA less than 13° , far less than was measured in the present study. Ali shows good agreement at low AoA. Yasuda did not measure the pitching moment.

The effect of spin on the loads is shown in Fig. 8 with curves for a consistent set of advance ratios (AdvR 0 to 1.04) presented on each plot. The positive and negative

load components are defined with reference to the conventional body fixed axes definition as depicted in Fig 1b, for a disc-wing rotating in the positive yaw direction.

The first thing to note is that the side force and rolling moment, for the non-spinning case i.e. AdvR = 0 (Fig. 8a&c), is essentially zero throughout the AoA range. This is as expected for a symmetrical, non-rotating body such as the disc-wing.

From previous work, the lift and drag curves overlay each other¹⁷ for all AdvR 0 to 1.04, which confirms that the lift and drag are unaffected by spin. The effect of spin on the side force, pitching moment and rolling moment (Fig. 8) is small but measurable. The side force (Fig. 8a) is zero throughout the AoA range for low AdvR 0 to 0.35 but for higher AdvR 0.69 & 1.04 becomes positive. The side force is approximately uniform across the entire AoA range, $C_Y = 0.04$ & 0.08 for AdvR of 0.69 & 1.04, respectively. The aerodynamic moments (Fig. 8b&c) exhibit similar characteristics, for low AdvR 0 to 0.35 the pitching and rolling moments remain unchanged. However for higher AdvR 0.69 & 1.04 both moments become more negative for typical flight angles of attack, 0° to 10° . The higher advance ratios 0.69 & 1.04 provide a greater nose down pitching moment (Fig. 8b) and a higher trim AoA just above 10° . The rolling moment is zero throughout the AoA range for low AdvR 0 to 0.35 (Fig. 8c) but for higher AdvR 0.69 & 1.04 becomes negative, $C_R = 0.006$ & 0.012 at 0° AoA for AdvR of 0.69 & 1.04, respectively.

The unstable pitching moment should render the disc-wing useless for sports disc applications. However, recall at this point that the rotating disc-wing is a flying gyroscope i.e. aerodynamic moments cause rotating motion perpendicular to the moment itself. This results in the pitching moment being de-coupled from the pitch leaving the AoA unaffected and instead causes roll divergence. Therefore, spin-stabilisation allows the disc to fly with acceptable (precessional) roll divergence, achieved with carefully designed mass distribution for the desired angular momentum requirements. The disc will never be stable in the sense that it will not return to its original aerodynamic orientation when disturbed. However, the favourable mass distribution of the disc i.e. weighted circumference, coupled with the rotation, maximises the angular momentum within the system so that the disc exhibits quite remarkable resistance to angular motion. The pitching moment for typical flight angles of attack (0° to 10°) has minimum gradient (0.001 per degree) and magnitude ($-0.01 < C_M < 0.004$) which in turn generates minimum precessional roll

motion. This minimises the roll divergence to within acceptable levels so that the disc is ‘quasi-stable’ or spin-stabilised. For high advance ratios (above 0.35) the greater nose down pitching moment (Fig. 8b) increases the roll divergence but still remains at an acceptable level.

The (precessional) pitch divergence is therefore caused by the spin-dependent Magnus rolling moment⁵ and has been shown to be zero for all typical flight AoA except for higher advance ratios, approaching 1 (Fig. 8c). At this speed (20m/s) the rotation rate would have to be 480rpm or above to start generating a non-zero rolling moment. Therefore, for a disc flying with low spin rates, the pitch divergence will be negligible.

The aerodynamic Robins-Magnus side force and Magnus rolling moment act on the spinning disc-wing due to the interaction of near surface fluid structures. For discussion of the fluid mechanics the reader is referred to Ref. 30. The resultant side force will not be an issue for low advance ratios. However, the disc may be required to fly at higher AdvR above 0.35. In this eventuality the disc may drift sideways in level flight or sideslip towards ground when flying with non-zero bank angle.

The late stall of the disc-wing is a typical low aspect ratio wing characteristic. Fluidically, the two wing tip trailing vortices are in very close proximity to one another¹⁸, due to the low aspect ratio, and together drive a strong central downwash which reattaches the separated shear layer up to 45° AoA^{3,18}. This provides the unique ability to fly at low speeds and very high angles of attack. The disc is commonly seen to almost hover at the end of its flight as it returns to ground with minimum vertical velocity, utilising these high AoA characteristics.

Surface Flow Visualisation

Visualisation of the flow over the upper and lower surfaces of the disc at zero angle of attack is shown in Fig. 9. The upper surface pattern (Fig. 9a) shows that the surface flow direction is from the leading edge towards L_1 , indicated by the streak lines within region A. The boundary layer separates from the surface leaving a clearly visible line (L_1) and the shear layer reattaches at L_2 . The boundary layer remains attached throughout region C and then separates off the surface at L_3 . A separation bubble is formed with reversed flow (from L_2 to L_1) on the surface and re-circulation within region B. From the trailing edge, a reversed surface flow pattern is observed within region D, as fluid is drawn towards the stagnation line at L_3 . Two nodes at the points V_1, V_2 indicate where trailing vortices detach from the surface. Streak lines in the vicinity of V_1, V_2

suggest that fluid from the separation bubble and from beneath the cavity feeds into these vortices.

The cavity surface pattern (Fig. 9b) indicates that the boundary layer separates off the leading edge lip and impinges on the inside of the trailing edge rim leaving a stagnation line (which cannot be seen on Fig. 9b). Reversed flow (F) exists from the trailing edge towards the stagnation line L_4 . The shear layer encloses a weakly circulating separation bubble (E).

Surface Pressure Distribution

The surface pressure distributions for a non-spinning disc were plotted from measurements taken at $Re = 2.84 \times 10^5$, equivalent to a flow speed of 15m/s and $AoA = 5^\circ$. The data is presented as colour weighted contour plots of pressure coefficients C_p and a cross-sectional profile for both the upper and lower (cavity) surfaces.

The data plotted in Fig. 10 takes the 3D surface pressure distribution and creates a 2D flat surface. Using the distance along the 3D surface profile from the disc centre, as the 2D radial distance (Fig. 10), for positional distances for the pressure points. The data is taken over the entire surface, to identify the symmetry of the pressure surface, not over half the disc and mirrored to the other side. The highest pressure region (red) occurs on the leading edge rim of the upper surface (Fig. 10a), the rim defined as the curved section of the disc. There is a low pressure crescent region (blue) aft of this high pressure region. The central part of the disc shows pressure recovery (green). The low pressure band (blue) on the trailing edge rim are associated with trailing vortices and bluff body effects. Low pressure (green) is seen within the cavity (Fig. 10b) except inside the trailing edge rim (red).

The data plotted in Fig. 11 meshes the pressure distribution onto the 3D disc shape (Fig. 11a) to show how it relates to the 3D geometry (Fig. 11b). The flow direction is from right to left, depicting the pressure distribution in 3D as described above.

The central cross-sectional pressure profile at the half span station is shown in Fig. 12, leading edge on the left of the figure. The upper surface is shown by the unbroken line, the lower surface curve is dashed. The cross-sectional disc geometry is also shown to relate the location of pressure peaks to the disc surface. The high (positive) pressure coefficient on the leading edge is shown by the spike at zero chord ($C_p \rightarrow 1$), positive pressure axis down. The lowest pressure region at around tenth chord ($C_p = -1.25$) and secondary peak thereafter produce a large suction on the leading edge. The pressure recovery on the upper surface is the same pressure as in the cavity ($C_p = -0.25$) through the central

portion (0.3c to 0.6c). The high pressure trough in the cavity ($C_p = 0.3$) and the upper surface low pressure peak ($C_p = -0.8$) are shown on the trailing edge. It is clear that the main contributions to the lift are from the low pressure peak on the leading edge and the large pressure difference on the trailing edge. From an approximate area rule it can be seen that the pitching moment is well balanced but slightly nose down (negative).

Comparison of Pressure Distribution & Surface Flow

The flow structures over a flying disc are related to the surface pressure distribution. The comparison images of Fig. 13 are the half surface 3D pressure distribution, viewed perpendicular to the surface, superimposed onto the half surface flow visualisation images. The separation line, on the upper surface (Fig. 13a), is seen to be just aft of the lowest pressure (blue) region on the leading edge. The reattachment is responsible for the pressure recovery (green). The trailing edge separation and nodes correspond to the low pressure (blue) band on the trailing edge and are very similar in form. The high pressure region on the trailing edge, within the cavity (Fig. 13b), corresponds to the point where the separated shear layer impinges inside the rim. The rest of the pressure cavity shows suction beneath the shear layer. The straight surface paint line defining the boundary between these two regions is not visible in the pressure data (Fig. 13b) in this highly turbulent environment.

Smoke Wire Flow Visualisation

The flow structures on the upper surface planform were visualised using the smoke wire method at 0° AoA. The separation bubble is clearly identifiable for the non-spinning case (Fig. 14, top), note the symmetry particularly in the wake. For the spinning case (Fig. 14, bottom) the form of the separation bubble is largely unchanged however the bubble shifts slightly towards the leading edge on the advancing side (left of the figure) and towards the trailing edge on the retreating side. Also, the fluid within the bubble is curved around the leading edge with the local surface and is mostly shed from the retreating side. The wake becomes asymmetric and is deflected slightly towards the advancing side.

The cross-section of the trailing vortices is shown at 10° AoA in Fig. 15, illuminated by a laser light sheet. The symmetrical vortices (top) for the non-spinning disc become asymmetric for increased rotation (middle through bottom). The advancing side of the disc, on the left side of each image, inhibits the near surface flow (for non-zero advance ratio) and retards the downwash on that side destroying the vorticity given to the trailing vortex. Whereas the retreating side of the disc, on the

right hand side of each image, aides the near surface flow (for non-zero advance ratio) and augments the downwash on that side enhancing the vorticity given to the trailing vortex.

The reader is referred to Ref. 18 for the proposed flow topology for the non-spinning case, for 10° AoA.

Flying Disc Dynamics

A flying sports disc generates lift through forward velocity just like a conventional wing. The lift contributed by spin is insignificant and does not provide nearly enough down force to support hover. Without spin, the disc tumbles ground-ward under the influence of an unstable aerodynamic pitching moment. From a backhand throw however, spin is naturally given to the disc. The unchanged pitching moment now results in roll, due to gyroscopic precession, stabilising the disc in free-flight.

The typical S shaped flightpath exhibited from a back-hand throw is dictated by the pitching moment. The angle of attack increases over the flight duration causing the disc to move through the zero pitching moment trim condition, close to 10° AoA. For a right-handed throw, the negative pitching moment on release causes the disc to roll (gyroscopic precession) and bank right, whereas late in the flight the positive pitching moment causes the disc to bank left. The reverse is true if the direction of spin is in the opposite direction e.g. from a left-handed throw, that is bank left early and right late on in the flight duration. It is important to stress that the pitching moment is small, approaching negligible for the majority of the flight. The rolling moment is negligible for the majority of the flight, the advance ratio increases over the flight duration approaching small non-zero rolling moments very late on. This means that the pitch attitude remains largely unchanged for the duration of the flight.

Conclusions

The combination of load data, surface pressure measurements and flow visualisation images has enabled the specification of flying disc aerodynamics and associated flow physics.

The aerodynamic load data agrees well with previous research found in the literature including linear lift and parabolic drag.

The pitching moment is unstable but small for typical flight angles of attack, resulting in a slight destabilising roll motion due to gyroscopic precession. The effect of spin on the aerodynamic loads is small, most notably causing a non-zero rolling moment and side force.

The surface pressure measurements for the non-spinning case reveal a surface distribution that agrees well with the flow visualisation, strengthening the description of the flow physics. The main contributions to the lift are from the low pressure peak on the leading edge and the large pressure difference on the trailing edge. The pressure profile suggests the pitching moment is close to zero but slightly nose down.

The flow visualisation has provided information for the explanation of the flow physics. The upper surface flow is characterised by an arc separation line on the leading edge rim, followed by an arc shaped reattachment. The cavity flow is characterised by separation at the leading edge lip and reattachment inside the trailing edge rim. Reversed flow occurs within the cavity forming a straight stagnation line.

The effect of spin causes slight asymmetries in the flow structures visible within the wake. The vorticity given to the trailing vortices is diminished and enhanced on the advancing and retreating side, respectively.

The typical S shaped flightpath exhibited from a back-hand throw is dictated by the pitching moment. For a right-handed throw, the negative pitching moment on release causes the disc to roll (gyroscopic precession) and bank right, whereas late in the flight the positive pitching moment causes the disc to bank left.

The high stall AoA provides the unique ability to fly at low speeds and very high angles of attack. The disc is commonly seen to almost hover at the end of its flight as it returns to ground with minimum vertical velocity, utilising these high AoA characteristics.

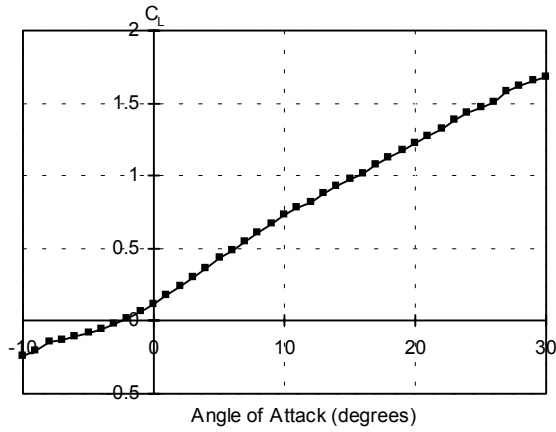
The reduced drag and increased lift of the intermediate shape would suggest superior performance but the larger (nose up) pitching moment would give stronger roll divergence. The profile drag of the flat plate disc is tiny but the pitching moment is even larger than the intermediate disc. The frisbee-like shape is the most favourable for use as a flying sports disc due to the minimum pitching moment gradient for the typical flight AoA range.

Acknowledgements

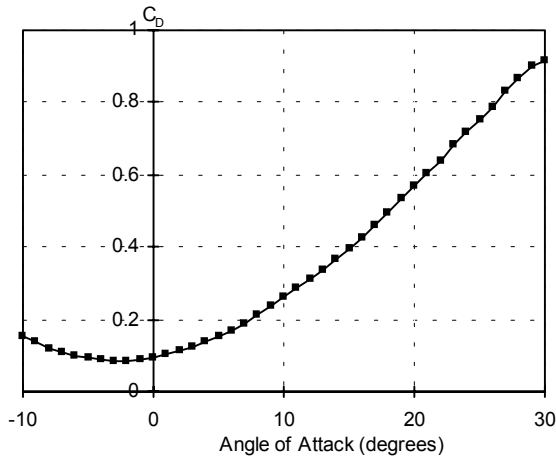
The authors would like to thank D. Mould at the Goldstein Research Laboratory for the skilled construction of the rig & disc. This research was funded by the EPSRC, award reference number 98317373.

References

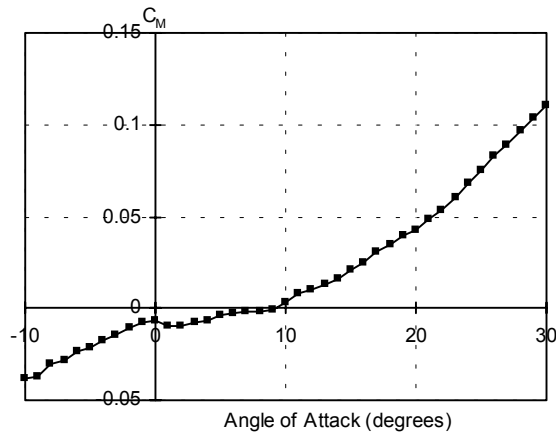
- (1) Johnson S.E.D., Frisbee, A Practitioner's Manual and Definitive Treatise, Workman Publishing Co., New York, 1975.
- (2) Headrick E.E., Flying Saucer, Patent Application, No. 3359678, Patented 26th Dec. 1967.
- (3) Potts J.R. & Crowther W.J., Disc-wing UAV: A Feasibility Study in Aerodynamics & Control, CEAS Aerospace Aerodynamics Research Conference, Cambridge, UK, June 2002.
- (4) Stilley G.D. & Carstens D.L., Adaptation of Frisbee Flight Principle to Delivery of Special Ordnance, AIAA 72-982, AIAA 2nd Atmospheric Flight Mechanics Conference, Palo Alto, California, USA, Sept. 1972.
- (5) Stilley G.D., Aerodynamic Analysis of the Self-suspended Flare, Honeywell Inc., NAD/Crane RDTR No.199, AD740117, 23 Feb. 1972.
- (6) Lazzara S., Schweitzer C. & Toscano, J., Design and Testing of a Frisbee Wind Tunnel Balance, Unpublished Report, Code: Engin 12, Brown University, Advisor: Prof. Karlson S.K.F., May 1980.
- (7) Mitchell T.L., The Aerodynamic Response of Airborne Discs, MS Thesis, University of Nevada, Las Vegas, NV, USA, 1999.
- (8) Ali W., Aerodynamics of Rotating Disc Wings, Division of Aerospace, Undergraduate Report, School of Engineering, University of Manchester, UK, April 1998.
- (9) Cotroneo P.W., Biomechanical and Aerodynamical Aspects of the Backhand and Sidearm Frisbee-Disc Throws for Distance, MS Thesis, Faculty of Phys. Ed., Cal. State Univ., Hayward, June 1980.
- (10) Lissaman P.B.S., Disc Flight Dynamics, Unpublished Document, University of Southern California, 29th Dec. 1998.
- (11) Lissaman P.B.S., Stability and Dynamics of a Spinning Oblate Spheroid, Unpublished Document, University of Southern California, 2th Dec. 1994.
- (12) Lissaman P.B.S., Range of a Free Disc, Unpublished Document, University of Southern California, 4th Jan. 2001.
- (13) Katz P., The Free Flight of a Rotating Disc, *Isreal J. Tech.*, Vol. 6, No. 1-2, 1968, pp150-155.
- (14) Hubbard M. & Hummel S., Simulation of Frisbee Flight, 5th Conf. on Mathematics and Computers in Sport, G. Cohen (Ed.), University of Technology, Sydney, Australia, June 2000.
- (15) Hummel S. & Hubbard M., Identification of Frisbee Aerodynamic Coefficients using Flight Data, 4th International Conference on the Engineering of Sport, Kyoto, Japan, Sept. 2002.
- (16) Hummel S. & Hubbard M., A Musculoskeletal Model for the Backhand Frisbee Throw, 8th International Symposium on Computer Simulation in Biomechanics, Politecnico di Milano, Milan, Italy, July 2001.
- (17) Potts J.R. & Crowther W.J., The Flow Over a Rotating Disc-wing, RAeS Aerodynamics Research Conference Proc., London, UK, Apr. 2000.
- (18) Potts J.R. & Crowther W.J., Visualisation of the Flow Over a Disc-wing. Proc. of the Ninth International Symposium on Flow Visualization, Edinburgh, Scotland, UK, Aug. 2000.
- (19) Potts J.R. & Crowther W.J., Application of Flow Control to a Disc-wing UAV, 16th UAV Systems Conference, Bristol, UK, April 2001.
- (20) Potts J.R. & Crowther W.J., Flight Control of a Spin Stabilised Axi-symmetric Disc-wing, AIAA 2001-0253, 39th Aero. Sci. Meet & Exhibit, Reno, NV, Jan. 2001.
- (21) Higuchi H., Goto Y., Hiramoto R. & Meisel I., Rotating Flying Disks and Formation of Trailing Vortices, AIAA 2000-4001, 18th AIAA Applied Aero. Conf., Denver, CO, Aug. 2000.
- (22) Yasuda K., Flight- and Aerodynamic Characteristics of a Flying Disk, *Japanese Soc. Aero. Space Sci.*, Vol. 47, No. 547, pp 16-22, 1999 (in Japanese).
- (23) Nakamura Y. & Fukamachi N., Visualisation of Flow Past a Frisbee, *Fluid Dyn. Res.*, v7, pp31-35, 1991.
- (24) Pozzy T., Getting More Distance - How Important Is Disc Speed, *Disc Golf World News*, No. 57, Spring 2002.
- (25) Pozzy T., Getting More Distance - How The Pros Do It, *Disc Golf World News*, No. 60, Winter 2002.
- (26) Zdravkovich M.M., Flaherty A.J., Pahle M.G. & Skelhorne I.A., Some Aerodynamic Aspects of Coin-like Cylinders, *JFM*, v360, pp73-84, 1998.
- (27) Ganslen R.V., Aerodynamic and Mechanical Forces in Discus Flight, *Athletic J.*, Vol. 44, Pages 50, 52, 68 & 88-89, 1964.
- (28) Tutjowitsch V.N., *Theorie der Sportlichen Wurfe Teil 1, Leistungssport*, Vol. 7, pp. 1-161, 1976.
- (29) Kentzer C.P. & Hromas L.A., Letter to: Mr. Willis B.E. (Unpublished Research Report), School Aero. Eng., Purdue University, Lafayette, Indiana, USA, 2nd July 1958.
- (30) Potts J.R., Disc-wing Aerodynamics, PhD Thesis, University of Manchester, UK, 2002.



(a) Lift coefficient.

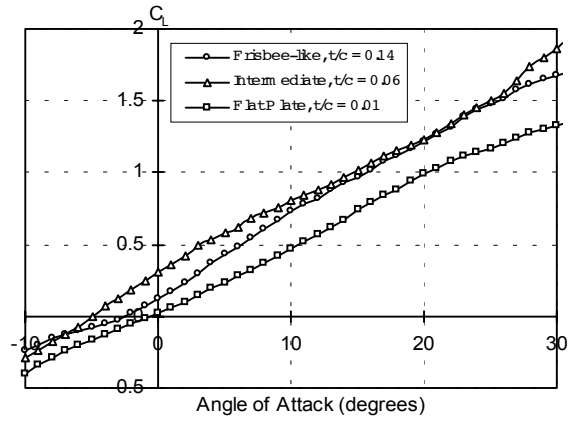


(b) Drag coefficient.

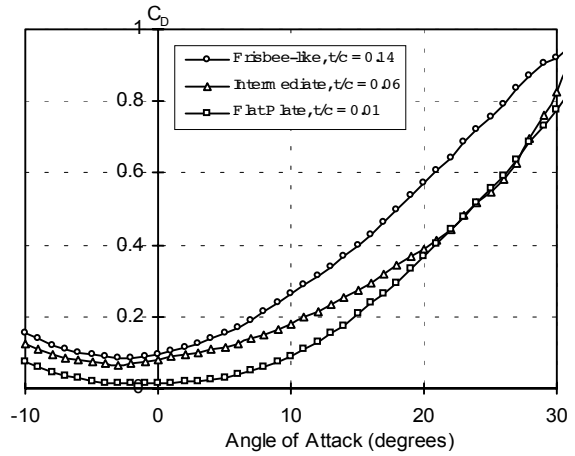


(c) Pitching moment coefficient.

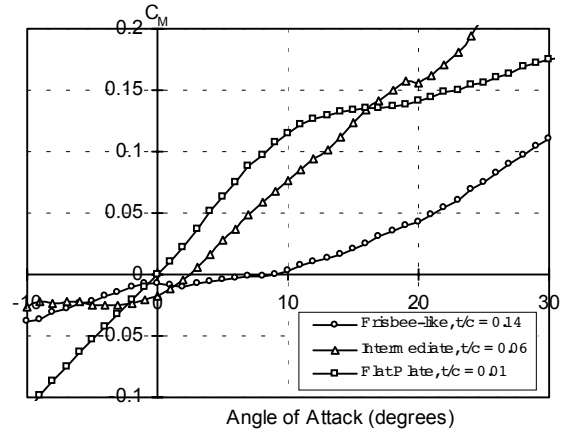
Fig. 5 Load characteristics at zero spin rate, $\text{AoA} = -10^\circ$ to 30° , $V = 20\text{m/s}$, $\text{Re} = 3.78 \times 10^5$.



(a) Lift coefficient.



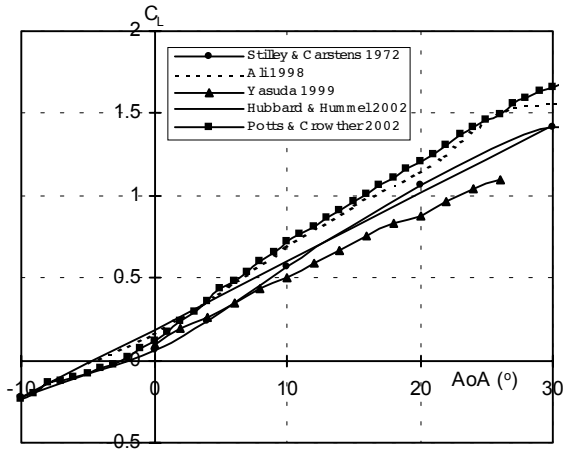
(b) Drag coefficient.



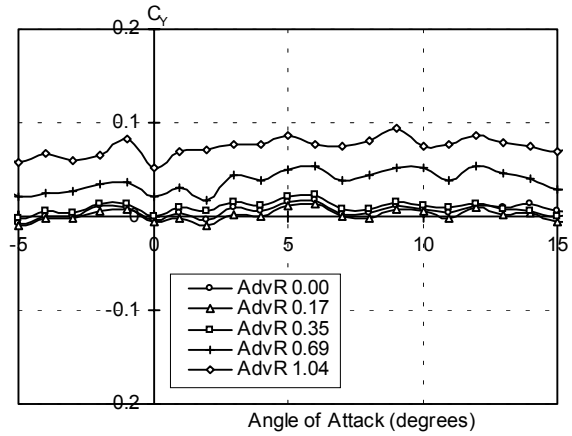
(c) Pitching moment coefficient.

Fig. 6 Load characteristics at zero spin rate, for three discs with various thicknesses $\text{AoA} = -10^\circ$ to 30° , $V = 20\text{m/s}$, $\text{Re} = 3.78 \times 10^5$.

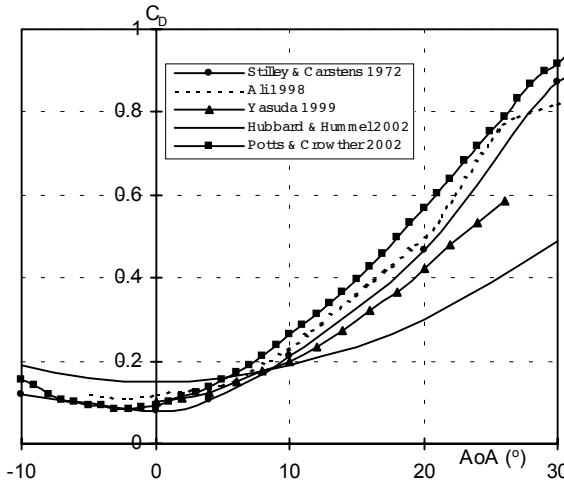




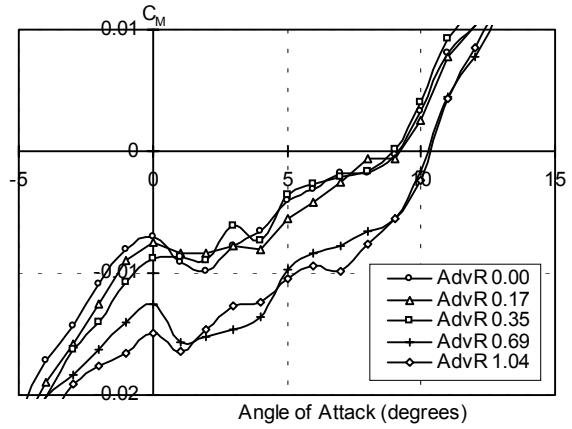
(a) Lift coefficient.



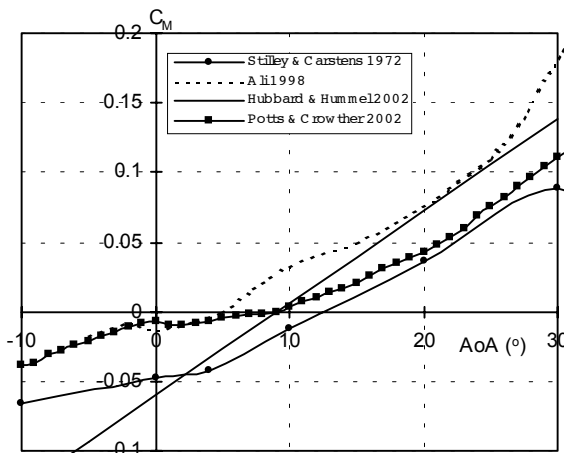
(a) Side force coefficient.



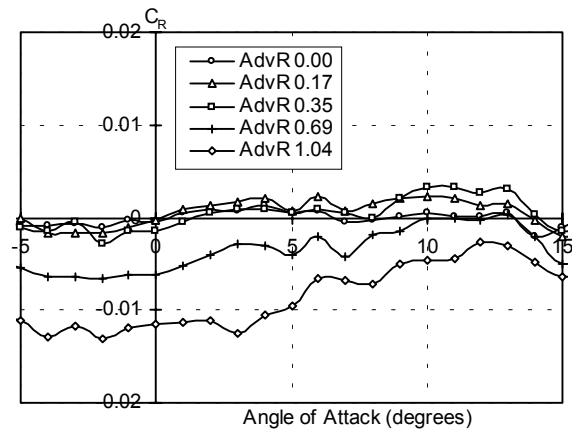
(b) Drag coefficient.



(b) Pitching moment coefficient.



(a) Pitching moment coefficient.



(c) Rolling moment coefficient.

Fig. 7 Comparison of load data to that found in literature for similar frisbee-like disc geometries, $AoA = -10^\circ$ to 30° .

Fig. 8 Load characteristics at various advance ratios, $AdvR = 0$ to 1 , $AoA = -5^\circ$ to 10° , $V = 20\text{m/s}$, $Re = 3.78 \times 10^5$.

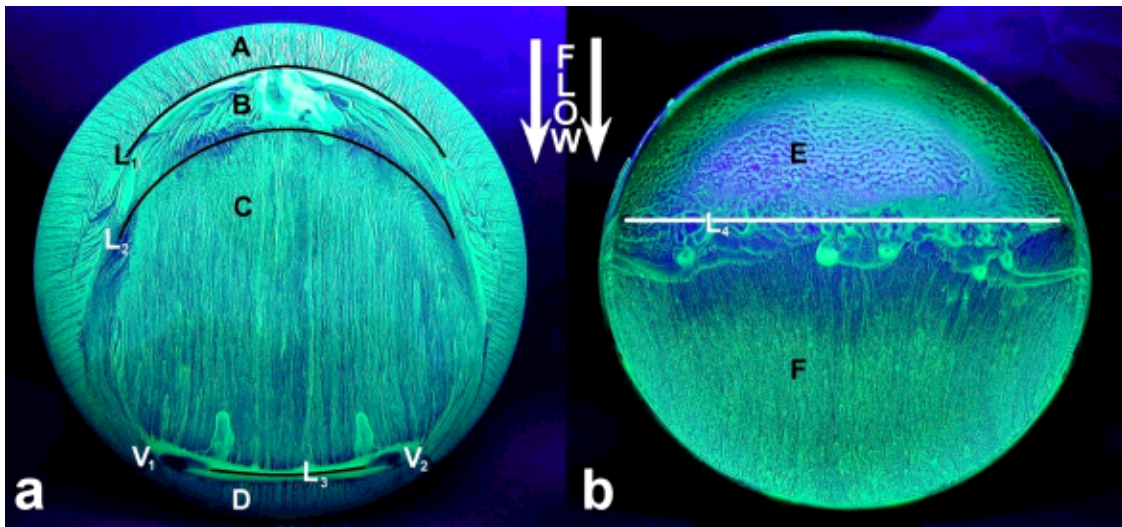


Fig. 9 The upper (a) and cavity (b) surface paint patterns at 5° AoA, $V = 15\text{m/s}$.

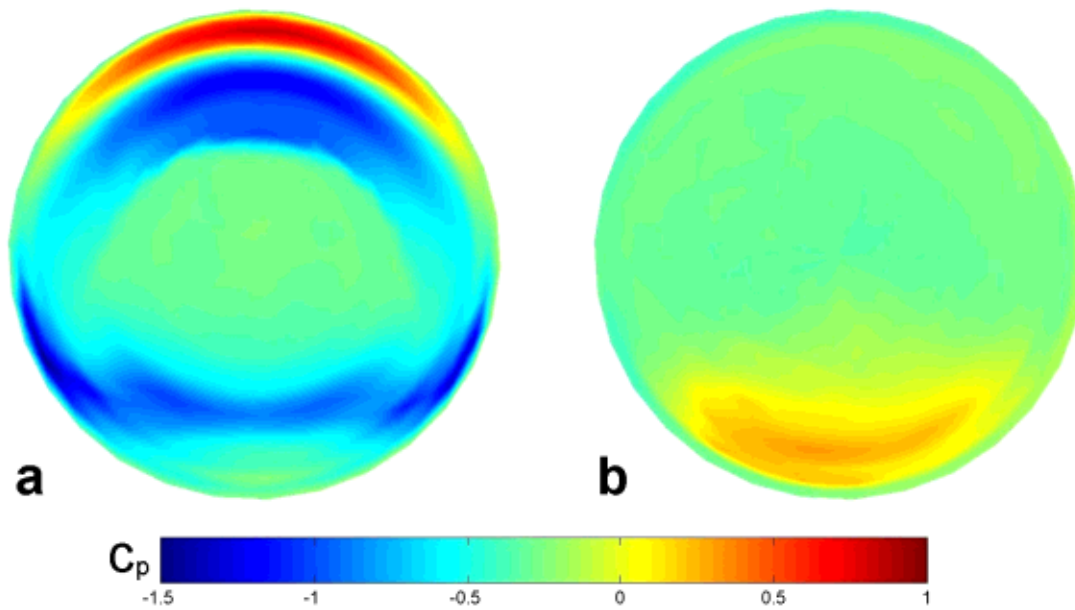


Fig. 10 Upper (a) and cavity (b) surface pressure distribution at 5° AoA, $V = 15\text{m/s}$.

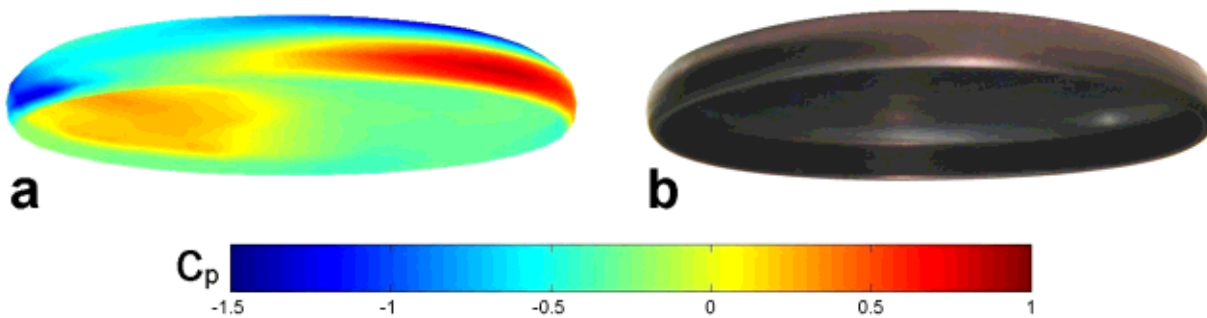


Fig. 11 (a) 3D surface pressure distribution at 5° AoA, $V = 15\text{m/s}$ (b) 3D disc geometry for comparison.

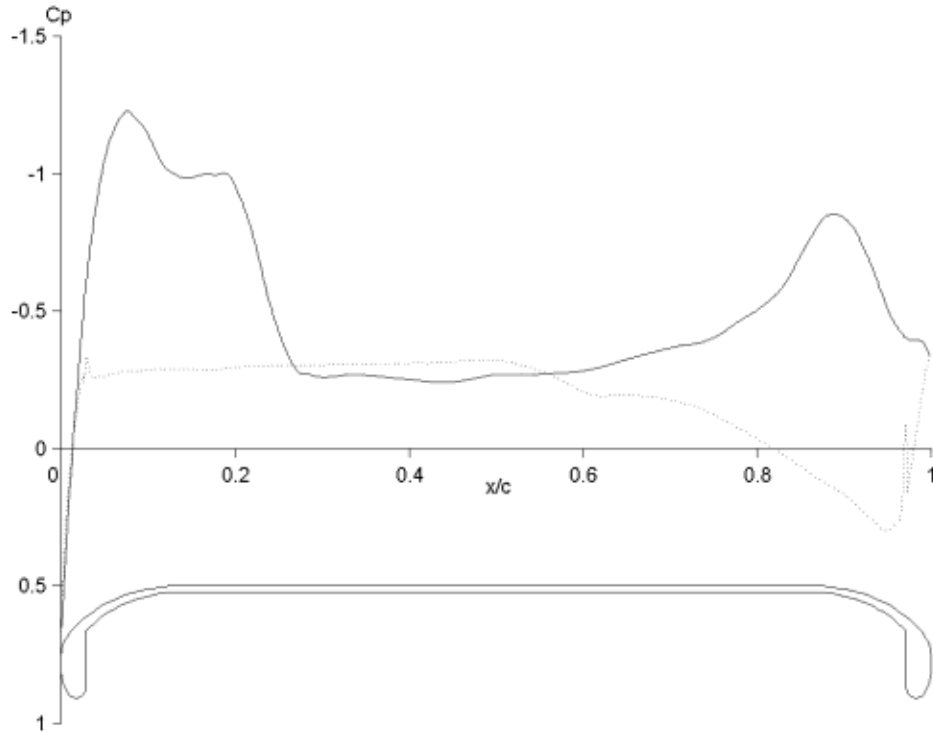


Fig. 12 Central cross-sectional pressure profile at half span station. Non-dimensional disc geometry shown below pressure plot, leading edge on the left of the figure. Unbroken line - upper surface, Dashed line - lower surface, 5° AoA, $V = 15\text{m/s}$.

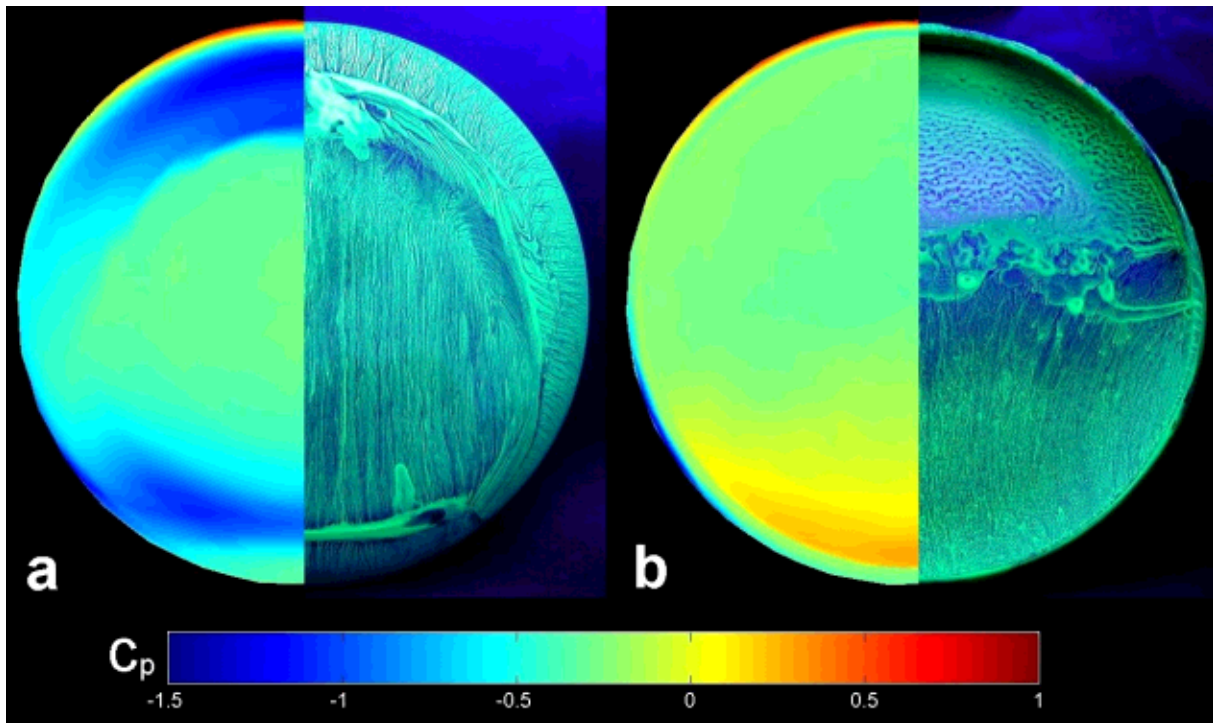


Fig. 13 Half surface 3D pressure distribution viewed perpendicular to the surface, superimposed onto the half surface flow visualisation images for the (a) upper and (b) cavity surface at 5° AoA, $V = 15\text{m/s}$.

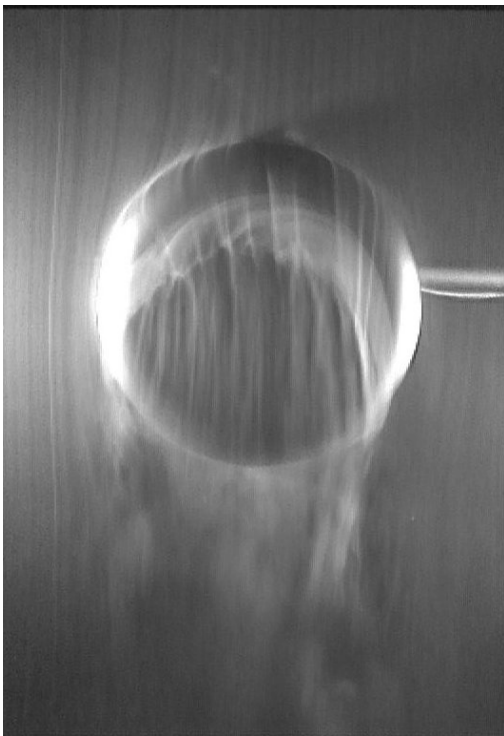
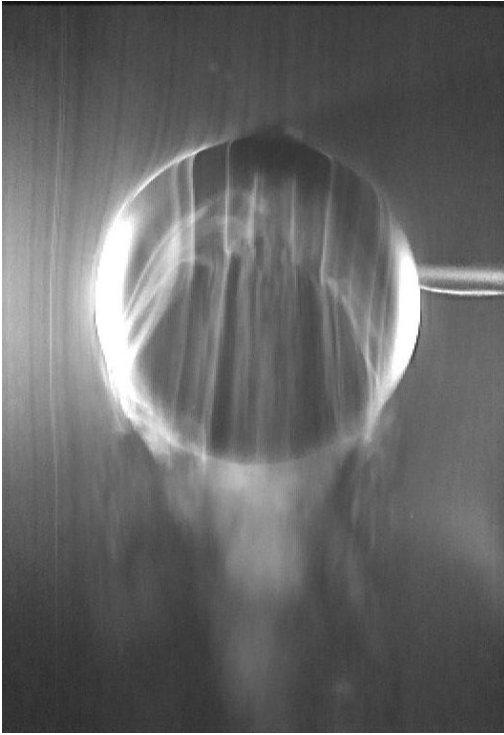


Fig. 14 Flow structures on the upper surface planform, for spin rates of (top) $AdvR = 0$, (bottom) $AdvR = 0.9$, 0° AoA, $V = 1.5\text{m/s}$. Advancing side on left of figure, retreating side on right.

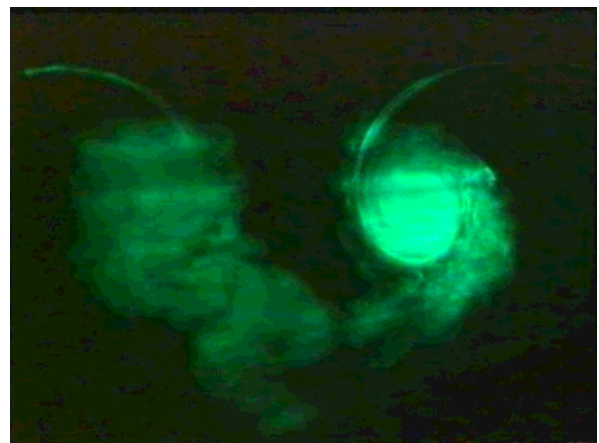
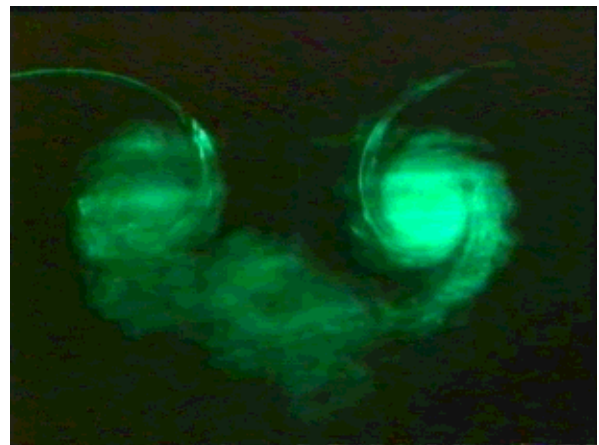
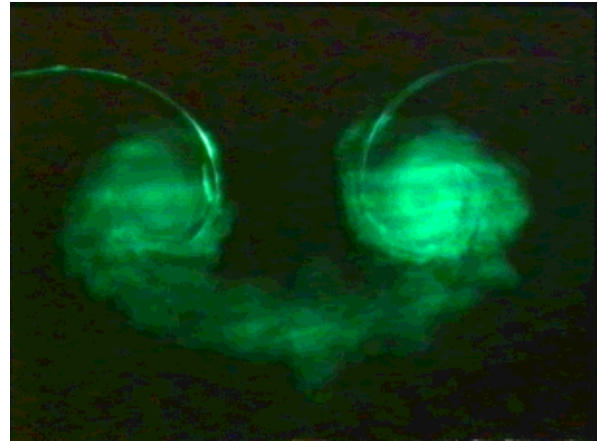


Fig. 15 Wake cross-section downstream from a flying disc, one diameter from the trailing edge for spin rates of (top) $AdvR=0$, (middle) $AdvR=0.7$ & (bottom) $AdvR=1.6$, 10° AoA, $V = 3\text{m/s}$. Advancing side on left of figure, retreating side on right.